ZAMM · Z. Angew. Math. Mech. **85**, No. 6, 400 – 410 (2005) / **DOI** 10.1002/zamm.200410193

Drop formation – an overview

Plenary lecture presented at the 75th Annual GAMM Conference, Dresden/Germany, 22–26 March 2004

Jens Eggers*

School of Mathematics, University of Bristol, University Walk, Bristol BS8 1TW, United Kingdom

Received 11 May 2004, accepted 19 January 2005
Published online 3 May 2005

Key words surface tension, free boundary problems, singularities
MSC (2000) 76D45, 35R35

We give a brief description of the technological challenges underlying the dynamics of drop formation, noting that a number of significant early advances are associated with the TH Dresden. In particular, to understand the size distribution of drops, one has to consider the non-linear dynamics leading up to the point where the radius of the fluid neck goes to zero. In this pinch-off region, both the neck shape and the velocity inside it are described by scaling laws, which we investigate from the point of view of dimensional analysis. We consider the crossover between different scaling regions, and briefly discuss more recent developments.

© 2005 WILEY-VCH Verlag GmbH & Co. KGaA, Weinheim

1 Introduction

The formation of drops is an extremely generic phenomenon, concomitant to almost any free-surface flow. The driving force behind the separation of drops is surface tension, which by definition is an energy per unit area. Surface tension thus favors configurations with a minimum surface area, i.e. spherical drops. The pathway a free surface flow takes to reach the locally optimal state of isolated, spherical drops is however extremely complicated in general. This is illustrated by Fig. 1, a photograph taken at the falls of the Rhine river near Schaffhausen. Above the falls one observes a mist of very small drops, which remain suspended in the air. Thus whatever the nature of the dynamics leading to breakup, it is associated with a broad spectrum of drop sizes.

Fig. 1 A mist of very small droplets hovers over the falls of the Rhein near Schaffhausen.

* e-mail: Jens.Eggers@bristol.ac.uk

© 2005 WILEY-VCH Verlag GmbH & Co. KGaA, Weinheim

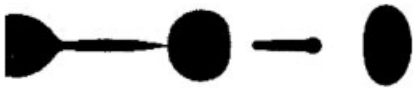

Fig. 2 Satellite formation in a water-glycerol jet [2].

Fig. 3 Cartoon of a hypothetical break-up mode without satellite formation.

What determines the drop size distribution in a spray is largely unknown and certainly depends on the character of the flow, but even the simplest possible case of the breakup of a cylindrical jet is non-trivial. The last stages of the breakup of a liquid jet are shown in Fig. 2. It is evident that there is not only one kind of drop produced in the process, but a much smaller, so-called "satellite" drop is formed from an elongated neck between two adjacent drops. The existence of the neck, in turn, is related to the fact that the profile near the point of break-up is extremely asymmetric: Toward the drop it is very steep, while toward the neck it is flat, forcing the neck into its slender shape. Thus the existence of satellite drops is intimately related to the non-linear properties of the fluid motion close to break-up, which produces the asymmetric shapes discussed above.

Drop formation of the type illustrated in Fig. 2 has extremely wide-ranging applications, as reviewed for example in [1]. The classical technique of ink-jet printing has been generalized to produce so-called microarrays for DNA analysis, to print integrated circuits, or to produce miniature lenses for optical applications. For all these applications it is very important to accurately control the size of the drop, thus satellite drops are detrimental to the quality, since they result in at least two *different* droplet sizes. It is therefore a natural question to ask whether it is possible to control the excitation of the jet leading to breakup, in such a way that only one type of drop is produced.

A desirable breakup configuration is illustrated schematically in Fig. 3. In an ideal situation the profile near breakup were symmetric, and breakup would occur in the middle between two drops. In that case the neck would snap back toward each of the drops, which would receive the same amount of mass, making all drops equal. It is one of the most important lessons of the non-linear dynamics of drop break-up that such a scenario is impossible: no matter how the jet is excited or what the initial condition may be, the pinch-off dynamics will always be the same, *independent* of initial conditions: the motion leading to breakup is universal.

2 Non-linear dynamics of drop formation

To obtain insight into the non-linear dynamics close to breakup one has to solve a notoriously difficult problem: the Navier-Stokes equation within a domain that is changing in time. The motion of the interface is dictated by the fluid motion itself, as the interface is convected passively by the fluid motion at the interface. The motion of the interface has to be computed with great accuracy, because the fluid motion is driven by surface tension, resulting in a Laplace pressure proportional to the mean curvature of the interface. Since the driving is proportional to pressure *gradients*, acceleration of a fluid element is effectively determined by *third derivatives* of the surface shape. The numerical difficulties inherent in this coupling of fluid motion and its driving force are discussed thoroughly in [3], giving an overview of available numerical methods.

To obtain greater insight into drop breakup, it is necessary to reduce the non-linear dynamics associated with it to its essentials. The idea is that near the point where the neck radius goes to zero, the fluid motion is directed primarily in a direction parallel to the axis. This allows to reduce the problem to an equation for the average velocity in the axial direction alone. Alternatively, and more or less equivalently, the velocity field can be expanded in the radial co-ordinate. If a typical radial length scale is smaller than the corresponding axial one, usually signaled by the interface slope being less than one, the leading order coefficient for the velocity suffices, as discussed in detail in [4]. Rather similar ideas were used, albeit in the framework of *linear* theory, by C. Weber [5], professor of hydraulics at the TH Dresden.

The result is a system of equations for the local radius $h(z,t)$ of the fluid neck, and the average velocity $v(z,t)$ in the axial direction. All other terms are of higher order in h or the radial variable r. For a liquid with kinematic viscosity ν, density ρ, and surface tension γ (neglecting the effect of the outer gas), the result of the calculation is:

$$\partial_t h^2 + \partial_z (v h^2) = 0\,, \tag{1}$$

$$\underbrace{\partial_t v + v\partial_z v}_{\text{inertia}} = \underbrace{-\frac{\gamma}{\rho}\partial_z\left(\frac{1}{R_1}+\frac{1}{R_2}\right)}_{\text{surface tension}} + \underbrace{3\nu\frac{\partial_z(\partial_z v h^2)}{h^2}}_{\text{viscosity}} + \underbrace{g}_{\text{gravity}}\,. \tag{2}$$

The simplification achieved by (1), (2) is enormous. Firstly, the dimension of the problem been reduced by one (the radial variable has been eliminated). Secondly, the moving boundary has been described explicitly by $h(z,t)$. Eq. (1) expresses the conservation of mass: It is written as a conservation equation for the volume $h^2 dz$ of a slice of fluid. Eq. (2) is a balance

© 2005 WILEY-VCH Verlag GmbH & Co. KGaA, Weinheim

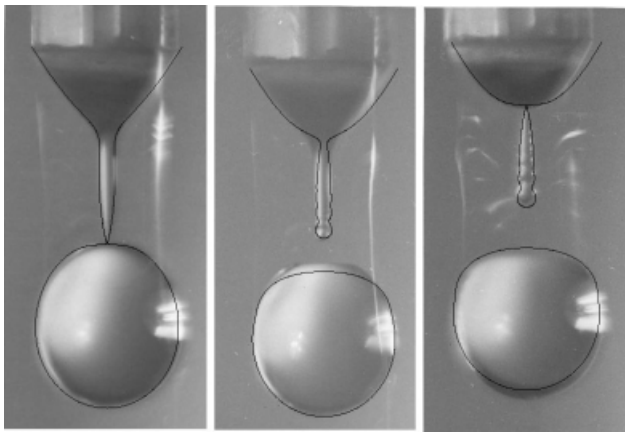

Fig. 4 A sequence of photographs showing a drop of water falling from a pipette $D = 5.2\,\mathrm{mm}$ in diameter [7]). The superimposed black lines are the result of a simulation of the one-dimensional eqs. (1), (2).

of forces acting on a fluid element, and thus very similar in structure to the original Navier-Stokes equation [6]. The l.h.s. of (2) corresponds to inertial forces, driven by surface tension, viscous forces, and gravity on the right. As to be expected from Laplace's formula, surface tension forces are proportional to the mean curvature, which for a body of rotation is

$$\frac{1}{R_1} + \frac{1}{R_2} = \frac{1}{h\sqrt{1+(\partial_z h)^2}} - \frac{\partial_{zz} h}{\sqrt{1+(\partial_z h)^2}^3}\,. \tag{3}$$

Strictly speaking, the radial expansion implied by (1), (2) would have required us to replace the mean curvature by the leading-order expression $1/h(z,t)$ alone. This is indeed sufficient to describe the neighborhood of the pinch point, but the applicability of the equations is greatly enhanced by including the full curvature, because the equations then include a spherical drop among its equilibrium solutions.

The remarkable power of the system (1), (2) in describing a real break-up event is illustrated by Fig. 4. The sequence of experimental pictures shows a drop of water falling from a pipette 5.2 mm in diameter. The drop is shown at the moment of the first bifurcation (first picture), after which the fluid neck recoils from the drop (second picture). Shortly afterward the neck pinches on its other end (third picture), thereby forming a satellite drop. It is evident from Fig. 4 that the one-dimensional approximation works extremely well in describing breakup, and the formation of satellite drops. This includes regions near the drop, where the profile is actually quite steep, so the expansion underlying (1), (2) is formally not valid. A careful assessment of the quality of one-dimensional approximations, achieved through comparison with accurate numerical simulations of the full Navier-Stokes equation, is given in [8].

3 Similarity solutions

We now turn to the immediate neighborhood of the pinch point, where separation occurs. It is interesting to consider this problem from the point of view of dimensional analysis of the parameters expected to play a significant role close to the point of breakup. The description of breakup will by necessity be local, so we write everything with respect to the point of breakup z_0, t_0 in space and time. The "critical parameters" of the problem, which vary over many orders of magnitude in the region of interest are thus $\Delta z = z - z_0$ and $\Delta t = t_0 - t$. At the singularity, they both go to zero.

By contrast, there are a number of parameters which remain fixed throughout the process. These are the fluid parameters ρ, ν, and γ, the radius R of the capillary, and the gravitational acceleration g. A lengthscale, which can quite reasonably be expected to be relevant as $\Delta t \to 0$, is the "diffusive" scale

$$\ell_t = \sqrt{\nu \Delta t}\,. \tag{4}$$

On the other hand, from the fluid parameters alone one can construct a length and a timescale which is "intrinsic" to the fluid motion:

$$\ell_\nu = \frac{\nu^2 \rho}{\gamma}\,, \qquad t_\nu = \frac{\nu^3 \rho^2}{\gamma^2}\,, \tag{5}$$

first introduced in A. Haenlein's dissertation [9] at the TH Dresden. As expected intuitively, length and time scales increase with viscosity, which can vary greatly between different fluids. For water, the viscous length scale ℓ_ν is just 10 nanometers, far below anything visible on the scale of the photographs in Fig. 4, while for glycerol, ℓ_ν is in the order of centimeters.

© 2005 WILEY-VCH Verlag GmbH & Co. KGaA, Weinheim

Using dimensional analysis [10], the profile h, which in its most general form reads

$$h = f(\Delta z, \Delta t, \rho, \nu, \gamma, g, R)\,, \tag{6}$$

may in fact be written

$$h = \ell_t \overline{f}(\Delta z/\ell_t, \ell_\nu/\ell_t, \ell_c/\ell_t, R/\ell_t)\,, \tag{7}$$

where all arguments of $\overline{f}$ are now *dimensionless*. In addition to the intrinsic length scale ℓ_ν, we have introduced the capillary length $\ell_c = \sqrt{\gamma/(\rho g)}$, set by the relative strength of capillary and gravitational forces.

To describe the singularity, we must study the limit that ℓ_t goes to zero. Anticipating that pinching is a local phenomenon, which cannot depend on any *external* scale like ℓ_c or R, we assume that the function $\overline{f}$ will remain finite in the limit that $\ell_c/\ell_t \to \infty$ and $R/\ell_t \to \infty$:

$$\begin{aligned} h &= \ell_t \overline{f}(\Delta z/\ell_t, \ell_\nu/\ell_t)\,, \\ v &= \frac{\ell_t}{\Delta t}\overline{g}(\Delta z/\ell_t, \ell_\nu/\ell_t)\,, \end{aligned} \tag{8}$$

making analogous assumptions about the velocity field. At this point, no further progress can be made on the basis of dimensional analysis alone, and a closer examination of of the equation of motion (2) is needed.

In a first step, we make the assumption that the pinch singularity is such that the fluid neck remains slender, i.e. that the slope $\partial_z h$ remains small. In this case the mean curvature can be approximated as $1/R_1 + 1/R_2 = 1/h$, which goes to infinity when h goes to zero: surface tension forces become very strong close to the singularity. In comparison, the constant gravity force g becomes diminutive, and will no longer be important near the singularity, so we obtain

$$\begin{aligned} &\partial_t \tilde{h}^2 + \partial_z(v\tilde{h}^2) = 0\,, \\ &\partial_t v + v\partial_z v = -\partial_z\left(\frac{1}{\tilde{h}}\right) + 3\nu\frac{\partial_z(\partial_z v\tilde{h}^2)}{\tilde{h}^2}\,. \end{aligned} \tag{9}$$

Here we have rescaled the height h as $\tilde{h} = h\rho/\gamma$, which leaves ν as the only parameter of the problem. In other words, γ and ρ can no longer appear in an expression for $\tilde{h}$ valid near the singularity. In terms of the parameters appearing in (8), this means that ℓ_ν drops out. Since $\tilde{h}$ has dimensions of cm^3/s^2, the only dimensionally consistent expression is

$$\begin{aligned} \tilde{h} &= \frac{(\Delta t)^2}{\ell_t^2} H(\Delta z/\ell_t)\,, \\ v &= \frac{\ell_t}{\Delta t} V(\Delta z/\ell_t)\,. \end{aligned} \tag{10}$$

Thus, using the additional scaling symmetry implicit in (9), we are able to completely fix the scaling form of the solution near the pinch point.

We have argued that gravity drops out of (2) to yield (9), and that the mean curvature simplifies to $1/h$. This can now be verified directly, using (10) to estimate all the terms appearing in (2). Namely, one finds

$$\partial_t v = \frac{\sqrt{\nu}}{2(\Delta t)^{3/2}}\left[V + \frac{\Delta z}{\ell_t}V'\right] \propto (\Delta t)^{-3/2}\,, \tag{11}$$

and similarly

$$v\partial_z v \sim \partial_z\left(\frac{1}{\tilde{h}}\right) \sim \frac{\partial_z(\partial_z v\tilde{h}^2)}{\tilde{h}^2} \propto (\Delta t)^{-3/2}\,. \tag{12}$$

Thus all terms appearing in the second equation of (9) are of the same order, blowing up rapidly as $\Delta t \to 0$. Inertial, surface tension, and viscous forces are all balanced at leading order. The gravitational acceleration g, on the other hand, is a constant and thus irrelevant close to pinch-off. The slope of the interface $\partial_z h$ scales like $(\Delta t)^{1/2}$, which means that the mean curvature reduces to the expression appropriate for a cylinder of radius h: $1/h$. The scaling solution (10), which we call the *Navier-Stokes solution*, thus represents a *dominant balance* of inertial, surface tension, and viscous forces. All other forces are small in comparison.

© 2005 WILEY-VCH Verlag GmbH & Co. KGaA, Weinheim

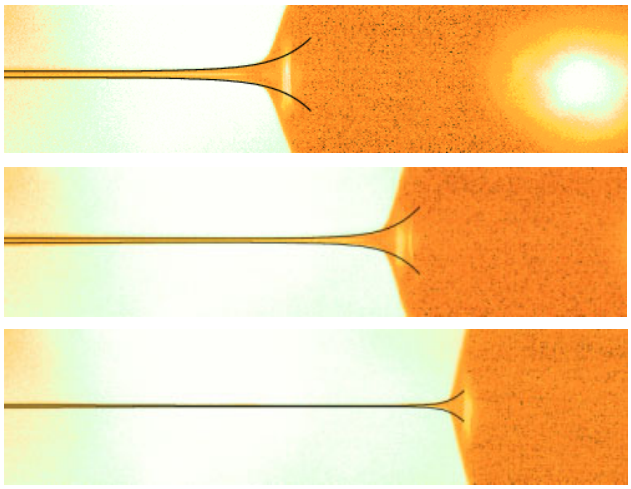

Fig. 5 A sequence of interface profiles of a jet of glycerol close to the point of breakup [12] (the center of the drop being formed is seen as a bright spot in the top picture). The experimental images correspond to $t_0 - t = 350\,\mu\text{s}$, $298\,\mu\text{s}$, and $46\,\mu\text{s}$ (from top to bottom). Corresponding analytical solutions based on (13) are superimposed [4].

Fig. 6 A drop of glycerol falling from a faucet [14].

Once the scaling form (10) is established, more progress can be made by inserting it into the set of partial differential eqs. (9), giving

$$\begin{aligned} -2H^2 + \xi H H' + (H^2 V)' &= 0\,, \\ V/2 + \xi V'/2 + VV' &= -(1/H)' + 3(V'H^2)/H^2\,, \end{aligned} \tag{13}$$

where the prime denotes differentiation with respect to the argument. This third-order system has to be solved using appropriate boundary conditions at infinity [11]. These are derived from the condition that matching must be possible to the macroscopic profile away from the singularity, which evolves on much longer timescales than the self-similar solution itself. Using the boundary conditions at infinity, it can be shown [4] that there is only one stable solution. A remarkable consequence of this universality is that the minimum neck radius, at a given time away from the point of breakup, is a quantity that is *independent* of the initial radius [4]:

$$h_{\min} = 0.03\,\frac{\gamma}{\nu\rho}(t_0 - t)\,. \tag{14}$$

To look at a comparison between theory and experiment in more detail, Fig. 5 shows three successive images of a jet of glycerol pinching off to form a drop (a small section of which is seen on the right). Once the temporal distance from the singularity is known (from experiment), the profile can be predicted without adjustable parameters (dark continuous lines). The only difference between the three sets of lines is that the axes have been rescaled by the factor implied by (10).

4 Transient regimes

The universality of the last stages of pinch-off seems to contradict observation: the pinch-off behavior of a low-viscosity fluid like water is quite different from that of a fluid possessing a high viscosity like glycerol. As can be seen in Fig. 4, the fluid neck of water has a conical form, while the bulbous shape of the drop is hardly disturbed. A very viscous fluid, on the other hand, shows a markedly different behavior, see Fig. 6. A very long thread is formed, which later breaks somewhere in the interior.

This seeming paradox is explained by the fact that depending on fluid parameters, different force balances may be realized *transiently*, while only the last stages of pinch-off are described by (10). Let us start with the case of very small viscosity, meaning that the viscous length scale ℓ_ν, relative to some external length scale like the nozzle radius R, is very small. Thus for the moment we consider the case of small Ohnesorge number [13] $Oh = \sqrt{\ell_\nu/R} \ll 1$, first introduced at the GAMM meeting of 1936 in Dresden.

© 2005 WILEY-VCH Verlag GmbH & Co. KGaA, Weinheim

Assuming that the limit $Oh \to 0$ is sufficiently regular, the only material parameter that can appear in an expression for $h(z,t)$ is the combination γ/ρ. Thus following the same logic as above, the only length scale that can appear in the solution close to pinch-off is the *inviscid* length scale [7]

$$\ell_{\rm in} = (\gamma \Delta t^2/\rho)^{1/3}\,. \tag{15}$$

Using dimensional analysis, and assuming as before that no outer scale like R or ℓ_c can enter the description of the local dynamics close to pinch-off,

$$\begin{aligned} h &= \ell_{\rm in} H_{\rm in}(\Delta z/\ell_{\rm in})\,,\\ v &= \frac{\ell_{\rm in}}{\Delta t} V_{\rm in}(\Delta z/\ell_{\rm in}) \end{aligned} \tag{16}$$

is the only possible form. For obvious reasons we call (16) the *Euler solution*. We have to add, though, that the true situation is bit more complicated since the full inviscid dynamics is not described by the the slender-jet eqs. (2). Indeed, it follows from (16) that the axial and the radial length scales of the solution are both $\ell_{\rm in}$, which means that that the basic assumptions underlying the derivation of (2) are not fulfilled. Instead, the full three-dimensional, axisymmetric equations of inviscid hydrodynamics must be solved, as was done in [15, 16]. The full Euler solution in fact reveals that the interface profile *turns over* very close to the pinch point, so the representation (16) is not uniformly valid, although this is immaterial to our dimensional argument.

We now turn to the case of large viscosities, which is characterized by $Oh \gg 1$. Continuing the logic of the previous paragraphs, we conclude that viscosity now dominates over inertia, which can be incorporated by putting $\rho = 0$. In this situation

$$\ell_{\rm vis} = v_\eta \Delta\, t \tag{17}$$

is the only local length scale, were $v_\eta = \gamma/\eta$ is the viscous velocity scale. Analogous to (16), this seems to imply that the similarity description of viscous pinch-off is

$$\begin{aligned} h &= \ell_{\rm vis} H_{\rm vis}(\Delta z/\ell_{\rm vis})\,,\\ v &= v_\eta V_{\rm vis}(\Delta z/\ell_{\rm vis})\,. \end{aligned} \tag{18}$$

However, we now show that this reasoning fails for the viscous case, and that the viscous solution is actually more complicated.

The reason is that in this particular case it was incorrect to assume that external scales like R or ℓ_c do not enter the description. This can be seen by putting $\rho = 0$ in (9), so that the second equation becomes

$$v_\eta \partial_z \left(\frac{1}{h}\right) = 3\,\frac{\partial_z(\partial_z v h^2)}{h^2}\,. \tag{19}$$

Multiplying (19) by h^2 and integrating once allows to express $v(z,t)$ in terms of $h(z,t)$, so that (9) becomes:

$$\begin{aligned} \partial_t h^2 + \partial_z(v h^2) &= 0\,,\\ 3\partial_z v/v_\eta &= C(t)/h^2 - 1/h\,, \end{aligned} \tag{20}$$

where the new function $C(t)$ only depends on time. It is easy to check that this set of equations is *invariant* under the transformation $z = a\tilde{z}$ and $v = a\tilde{v}$. Thus for any solution $h(z,t)$ of (20), there is another profile whose axial scale is stretched by an arbitrary factor a, so the local profile close to pinch-off *cannot* be universal.

Rather, there must be another length scale coming into the problem (ℓ_{ax}, say), whose value is set by the initial condition. In the case of the dripping tap discussed above, this scale will depend in some way on the external parameters: $\ell_{ax} = \ell_{ax}(R, \ell_c)$. But this means the assumptions underlying the scaling form (18) were not correct, and a dependence on ℓ_{ax} has to be taken into account. The invariance under the above transformation suggests to generalize (18) to

$$\begin{aligned} h &= \ell_{\rm vis} H_{\rm vis}(\Delta z/(\ell_{\rm vis} a))\,,\\ v &= a v_\eta V_{\rm vis}(\Delta z/(\ell_{\rm vis} a))\,, \end{aligned} \tag{21}$$

where a is a function of $\ell_{\rm vis}/\ell_{ax}$. Close to the singularity, we still expect self-similar behavior, so a is a power-law of the dimensionless ratio $\ell_{\rm vis}/\ell_{ax}$:

$$a = (\ell_{\rm vis}/\ell_{ax})^{\beta-1}\,, \tag{22}$$

© 2005 WILEY-VCH Verlag GmbH & Co. KGaA, Weinheim

where β is a new exponent to be determined. As the last case to be considered here, we call (21), (22) the *Stokes solution*.

The non-trivial case $\beta \neq 1$ is what Barenblatt [10] has called "self-similarity of the second kind". It implies that the solution has a singular dependence on some outer parameter, associated with the appearance of a new exponent, which cannot be inferred from dimensional analysis or from symmetry considerations. Indeed, solutions of (20) which have the form (21,22) were first found in [17], here we will describe a simplification of the original calculation which allows β to be found analytically [4].

To this end, the set of eqs. (20) can be simplified enormously by going into a *Lagrangian* frame of reference $z(\alpha, t)$, where α labels a hypothetical particle, whose position is $z(\alpha, t)$ at time t. Since the motion is one-dimensional, Lagrangian paths can be found simply by integrating the relations

$$\partial_\alpha z = 1/h^2\,, \quad \partial_t z = v\,. \tag{23}$$

It is a simple matter to confirm that the relations (23) ensure that the first equation of (20), expressing mass conservation, is valid identically. From (23) follows the transformation law $\partial_z = (\partial_\alpha z)^{-1}\partial_\alpha$, which transforms the second equation of (20) into

$$\hat{h} - 6v_\eta \partial_t \hat{h}\hat{h} = C(t)\,, \tag{24}$$

where the variable $\hat{h}$ is the height in Lagrangian coordinates: $\hat{h}(\alpha, t) = h(z(\alpha, t), t)$. Remarkably, all spatial derivatives have dropped out of this equation, which again confirms the invariance under a rescaling of the axis. Self-similar solutions of (24) corresponding to (21), (22) are

$$\hat{h} = t'\chi(\zeta)\,, \qquad \zeta = \alpha'/t'^{2+\beta}\,, \qquad C = t'\overline{C}\,, \tag{25}$$

where $t' = v_\eta \Delta t/\ell_{ax}$ and $\alpha' = \alpha/\ell_{ax}^3$ are dimensionless measures of the distance from the singularity. Inserting (25) into (24) leads to the similarity equation

$$\overline{C} = \chi + 6\chi^2 - 6(2+\beta)\zeta\chi'\chi\,. \tag{26}$$

The constant of integration can in fact be computed if one remembers that $\hat{h}^{-2} = \partial_\alpha z$, and therefore $\chi^{-2} = F'$ for a suitable $F(\zeta)$. Namely, dividing (26) by χ^4 it follows that $\overline{C}/\chi^4 - 1/\chi^3$ is a total derivative, and thus

$$\overline{C} = \frac{\int_{-\infty}^{\infty} \chi^{-3}(\zeta) d\zeta}{\int_{-\infty}^{\infty} \chi^{-4}(\zeta) d\zeta} \tag{27}$$

by integrating from $-\infty$ to ∞. For this we have to assume that χ grows sufficiently fast at infinity, which simply says that the fluid neck at the pinch point becomes arbitrarily thin.

Separating variables in (26), one finds

$$\ln\left|\frac{\zeta}{\bar{\zeta}}\right| = 6(2+\beta)\int_{\overline{\chi}}^{\chi} \frac{\zeta' d\zeta'}{6\zeta'^2 + \zeta' - \overline{C}}\,, \tag{28}$$

and thus

$$\left|\frac{\zeta}{\bar{\zeta}}\right|^{2/(2+\beta)} = \left|\frac{6\chi^2 - \chi - \overline{C}}{6\overline{\chi}^2 - \overline{\chi} - \overline{C}}\left(\frac{(\Gamma + 1 + 12\chi)(\Gamma - 1 - 12\overline{\chi})}{(\Gamma - 1 - 12\chi)(\Gamma + 1 + 12\overline{\chi})}\right)^{1/\Gamma}\right|\,, \tag{29}$$

where $\Gamma = \sqrt{1 + 24\overline{C}}$. We anticipate that the profile is *symmetric* around the pinch point, so that the expansion around the minimum is

$$\chi(\zeta) = \chi_0 + \zeta^2 + \chi_2\zeta^4 + \dots\,. \tag{30}$$

Here we have used the fact that there is an arbitrary scale factor in the axial scale, so we normalized the quadratic coefficient to one. Using $\overline{\chi} \to \chi_0$ as $\bar{\zeta} \to 0$ in (29), one finds that $6\chi_0^2 - \chi_0 - \overline{C} = 0$. Demanding in addition that powers of $\bar{\zeta}$ on both sides of (29) match, one arrives at $-2/(2+\beta) = -2 + 2/\Gamma$. Both equations are easily combined to give

$$\chi_0 = \frac{1}{12(1+\beta)} \quad \text{and} \quad \overline{C} = \frac{3+2\beta}{24(1+\beta)^2}\,. \tag{31}$$

© 2005 WILEY-VCH Verlag GmbH & Co. KGaA, Weinheim

This allows us to read the constraint (27) as an equation for β. First, using (31), eq. (29) reduces to

$$\zeta = \left(\frac{6(1+\beta)}{2+\beta}\right)^{(3+2\beta)/2} \left[\chi + \frac{3+2\beta}{12(1+\beta)}\right]^{(3+2\beta)/2} (\chi - \chi_0)^{1/2} . \tag{32}$$

Second, the integrals in (27) can be transformed using

$$\int_{-\infty}^{\infty} d\zeta/\chi^i = 2\int_{\chi_0}^{\infty} d\zeta/(\chi^i \chi') , \tag{33}$$

and inserting $\chi' = (\chi + 6\chi^2 - \overline{C})/(6(2+\beta)\zeta\chi)$. Evaluating the resulting integrals and using (31) gives

$$\frac{(1-\beta)(3+2\beta)}{(1+\beta)(3-2\beta)} = \frac{F(-1/2-\beta, 1-\beta; 3/2-\beta; -3-2\beta)}{F(-1/2-\beta, 2-\beta; 5/2-\beta; -3-2\beta)} , \tag{34}$$

which is the desired equation for β.

To obtain a numerical value for β, it is useful to remember a continued fraction representation for the hypergeometric function [18]:

$$\frac{F(a, b+1, c+1, z)}{F(a, b, c, z)} = c_0/(1 + c_1 z/1 + \ldots) ,$$

where

$$c_1 = 1 , \qquad c_{2n} = -\frac{(n+a)(n+c-b)}{(2n+c)(2n+c+1)} , \qquad c_{2n-1} = -\frac{(n+b)(n+c-a)}{(2n+c)(2n+c-1)} .$$

This leads to a rapidly converging representation of the right-hand-side of (34), which can be used to find the value of β numerically:

$$\beta = 0.174871700652042307111\ldots . \tag{35}$$

Thus in summary we have found the form of the profile in the viscously dominated case to be

$$h = \ell_{\rm vis} H_{\rm vis}(\Delta z \ell_{ax}^{\beta-1}/\ell_{\rm vis}^{\beta}) \tag{36}$$

which indeed depends on the external parameter ℓ_{ax} in a singular fashion. The small value of β implies that in the limit $\Delta t \to 0$ the solution is extremely long and slender, since $(\Delta t)^{\beta} \gg \Delta t$. This is consistent with the long thread seen in Fig. 6, although the stretching by the falling viscous drop, that is attached to it, also plays a significant role.

5 Crossover

So far we have found three different similarity solutions, corresponding to different balances between the three types of forces acting on a fluid element: inertia, surface tension, and viscosity. It is clear that surface tension must always appear, since it is responsible for driving the system toward pinch-off. However, it remains to be seen how the three different balances described so far fit together in a given experimental situation.

It is easiest to argue starting from the extreme cases of very high and very low Ohnesorge numbers. If the viscosity is very small, the viscous term is unimportant initially. Hence, once a similarity solution has developed, it follows the Euler scaling (16). Inserting the scaling form (16) into (9), one can estimate the relative size of the inertial and the viscous term, respectively. The inertial term scales like $\Delta t^{-4/3}$, the viscous term like $\Delta t^{-5/3}$, so in the limit $\Delta t \to 0$ viscosity can no longer be neglected, and the solution (16) must break down. Not surprisingly, this happens when

$$h_{\rm min}^{Eu \to NS} \approx \ell_{\nu} . \tag{37}$$

This result is confirmed by experiment as well as full numerical simulations of the Navier-Stokes equations [19]. At the minimum radius prescribed by (37), the similarity solution (16) crosses over to (10). Thus ultimately, at a sufficiently small scale, the Navier-Stokes scaling (10) will be seen. For low-viscosity fluids like water, however, ℓ_{ν} is only about $10nm$, so this crossover will be hard to be observed at all.

Turning now to the opposite case of $Oh \gg 1$, we can argue similarly that inertial terms will be unimportant relative to viscosity, so (21) will be observed. Inserting (21) into (9), we now find that $v\partial_z v \propto \Delta t^{\beta-2}$ and $\partial_z(\partial_z v h^2)/h^2 \propto \Delta t^{-\beta-1}$.

© 2005 WILEY-VCH Verlag GmbH & Co. KGaA, Weinheim

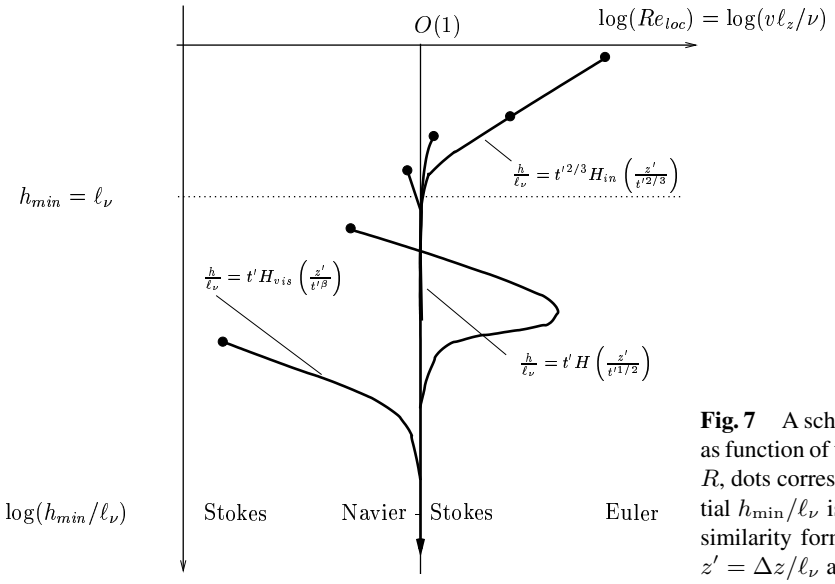

Fig. 7 A schematic of the trajectory the minimum radius takes as function of the local Reynolds number. At fixed nozzle radius R, dots correspond to different values of the viscosity. The initial $h_{\min}/\ell_\nu$ is approximately $R/\ell_\nu \approx Oh^2$. We also give the similarity form of solutions, using dimensionless coordinates $z' = \Delta z/\ell_\nu$ and $t' = \Delta t/t_\nu$.

This time the role of viscosity and inertia is reversed, and the latter will eventually take over, implying a crossover toward the Navier-Stokes solution (10). This qualitative observation has also been confirmed experimentally in [20].

The estimate of the crossover scale is more subtle in the viscous case, since the Stokes solution (21) itself is not completely universal, but depends on the parameter $\ell_{ax}^{\beta-1}$. The scale ℓ_{ax} might be estimated by matching it to the initial instability of, say, a drop falling from a tap. Once the interface is sufficiently deformed, i.e. when $h/R \approx r_c$, the motion is sufficiently non-linear for the similarity solution (21) to have established itself. This is consistent with experimental observation [20], where r_c is estimated to be 0.5. At this first transition, the longitudinal scale $\ell_{\rm vis}^{\beta}/\ell_{ax}^{\beta-1}$ must be comparable to the scale of the initial instability, which will be proportional to R itself. From this condition it follows that $\ell_{ax} \propto R$, i.e. the axial scale is set by R itself, and the Stokes similarity solution is

$$\begin{aligned} h &= \ell_{\rm vis} H_{\rm vis}(\Delta z R^{\beta-1}/\ell_{\rm vis}^{\beta})\,, \\ v &= (\ell_{\rm vis}/R)^{\beta}\, v_\eta V_{\rm vis}(\Delta z R^{\beta-1}/\ell_{\rm vis}^{\beta})\,. \end{aligned} \tag{38}$$

Now we can use (38) to find the condition for inertia and viscosity being comparable. We find the crossover scale between Stokes scaling (38) and Navier-Stokes scaling (10) to be

$$\frac{h_{\min}^{St\to NS}}{R} \approx \left(\frac{{\rm Re}_{\rm cr}\ell_\nu}{R}\right)^{1/(2\beta-1)}\,, \tag{39}$$

where ${\rm Re}_{\rm cr}$ is the critical value of the local Reynolds number where crossover occurs. Eq. (39) predicts that the minimum radius at which crossover occurs is strongly viscosity-dependent: $h_{\min}^{St\to NS} \propto \nu^{-3.08}$. Unfortunately, this scaling is not in agreement with experimental observation [20], where $h_{\min}^{St\to NS}$ to a good approximation was found to be *independent* of viscosity. Even when inserting ${\rm Re}_{\rm cr} \propto \nu^{-1}$, as was estimated in [20], this is not enough to account for the observed behavior of $h_{\min}^{St\to NS}$.

The reason for this discrepancy is unknown, but it might be related to the fact that the scaling function $H_{\rm vis}$ of (38) is symmetric, while the asymptotic profile H is highly asymmetric. Thus the crossover from one solution to the other involves the breaking of a symmetry, which could delay the transition: even if inertia is no longer small, this may not be enough to break the symmetry. As a result, the crossover region could be unusually broad, one similarity solution not merging directly into the other.

We can try to summarize the different types of scaling behavior and the crossover between them in a simple diagram. In a doubly logarithmic scaling, we have plotted the local Reynolds number on the abscissa, which measures the relative size of the inertia to viscosity at a given time in the evolution of the liquid bridge, where v is a typical velocity and ℓ_z a typical length scale in the axial direction. The minimum radius, non-dimensionalized by ℓ_ν, is on the ordinate. In a given experimental situation, characterized for example by a nozzle radius R, the evolution starts from different points in the diagram, marked by dots, depending on the viscosity of the test fluid. We have not attempted to accurately represent the initial dynamics, which is characterized by a linear instability, but rather focus on the scaling behavior.

© 2005 WILEY-VCH Verlag GmbH & Co. KGaA, Weinheim

For the Navier-Stokes solution, which balances all forces, $\mathrm{Re}_{\mathrm{loc}}$ evidently must be constant and of order 1. For large Ohnesorge number, pinching starts on the r.h.s of the diagram, where all solutions fall onto the same curve. When $h_{\min}$ reaches ℓ_ν, crossover toward the Navier-Stokes solution occurs. If the Ohnesorge number is small, the Stokes solution is followed first, and different trajectories form parallel lines. We have attempted to sketch the experimentally observed crossover behavior, which is that at moderate values of Oh the Reynolds number $\mathrm{Re}_{\mathrm{loc}}$ can become significantly higher than unity, before returning to its value appropriate for the Navier-Stokes solution.

6 Outlook

So far we have only considered cases where the outer fluid or gas maybe neglected. Strictly speaking, the outer fluid always becomes relevant at sufficiently small thread diameters, and the motion is described by Stokes' equation [21]. Owing to the long-ranged interactions transmitted by the outer fluid in Stokes flow, the similarity form (18) one might expect on dimensional grounds, gives *logarithmically diverging* contributions in the boundary integral description [22] of the problem. This leads to a novel type of similarity solution, in which scale invariance is broken by the presence of a logarithmic term [23]:

$$h = \ell_{\mathrm{vis}} H_{\mathrm{out}}(\Delta z/\ell_{\mathrm{vis}} + b\ln(\ell_{\mathrm{vis}}/R))\,. \tag{40}$$

Here R is some outer length scale that has to be introduced to keep the logarithm from diverging. The constant b is a universal number that is related the asymptotic slope H'_{out} of the interface at infinity. The similarity function H_{out} depends strongly on the ratio λ of the inner viscosity divided by the outer viscosity [24], and is always asymmetric. Evidently, this implies that the limit $\lambda \to \infty$ is singular, since H_{vis}, appropriate for the Stokes limit in the *absence* of an outer fluid, is symmetric. In fact, the solution (40) seems to become unstable at about $\lambda \approx 32$ [24]. Another interesting limiting case is $\lambda = 0$, i.e. that of a bubble of negligible viscosity in a viscous fluid [25]. In that situation the equations of motion become effectively *linear*, so H_{out} looses its most crucial characteristic of universality: its form depends on the initial conditions.

As the thickness of the fluid neck decreases, it becomes increasingly sensitive to noise, a fact first investigated both experimentally and theoretically in [14]. If the fluid is viscous, a non-linear instability can set in at a thread thickness of a few microns, as found experimentally in glycerol-water mixtures [12, 14]. This instability leads to the growth of secondary necks on the similarity solution (10), a process which can repeat itself several times on smaller and smaller scales [14]. If thermal fluctuations of the surface are the source of the noise, the thermal length scale

$$\ell_T = \sqrt{k_b T/\gamma}\,, \tag{41}$$

comes into play, where T is absolute temperature and k_B Boltzmann's constant. A typical value of ℓ_T is about a nanometer at room temperature. Estimates of the critical thread radius, at which thermal fluctuations become important, seem to underestimate its value. There is therefore the possibility that other sources of noise, such as inhomogeneities in the glycerol-water mixture, might contribute to the instability. A variant of the slender-jet eqs. (1), (2), which includes the influence of noise in a systematic fashion, has recently been derived in [26], opening the door to a more quantitative theoretical study. The same equations were used to study a jet of propane only 6 nanometers in diameter, using molecular dynamics simulations. On this scale, which is of the same order as ℓ_T itself, breakup is modified strongly by thermal fluctuations [26]. Typical breakup events become symmetric, replacing the asymmetric Navier-Stokes breakup to be expected for this range of parameters. This feature of nano-scale motion can be understood by properly incorporating the influence of noise into the similarity description [27].

We can conclude that individual pinching events of a Navier-Stokes fluid are fairly well understood. Many open questions remain however for the pinching of non-Newtonian fluids, as exemplified by solutions of long polymer chains in high and low viscosity solvents [28, 29].

Acknowledgements I am very grateful to A. Hinsberger for supplying me with Fig. 1, and for very useful discussions.

References

[1] O. A. Basaran, AIChE J. (USA) **48**, 1842–1848 (2002).
[2] B. Lopez, Ph.D. thesis, University of Grenoble (1998).
[3] R. Scardovelli and S. Zaleski, Annu. Rev. Fluid Mech. **31**, 567–603 (1999).
[4] J. Eggers, Rev. Mod. Phys. **69**, 865–929 (1997).
[5] C. Weber, Z. Angew. Math. Mech. **11**, 136–154 (1931).
[6] L. D. Landau and E. M. Lifshitz, Fluid Mechanics (Pergamon, Oxford, 1984).
[7] D. H. Peregrine, G. Shoker, and A. Symon, J. Fluid Mech. **212**, 25–39 (1990).

© 2005 WILEY-VCH Verlag GmbH & Co. KGaA, Weinheim

[8] B. Ambravaneswaran, E. D. Wilkes, and O. A. Basaran, Phys. Fluids **14**, 2606–2621 (2002).
[9] A. Haenlein, Forsch. auf dem Gebiete des Ingenieurwesens/Reihe A **2**, 139–149 (1931).
[10] G. I. Barenblatt, Scaling, Self-Similarity, and Intermedeate Asymptotics (Cambridge University Press, Cambridge, 1996).
[11] J. Eggers, Phys. Rev. Lett. **71**, 3458 (1993).
[12] T. A. Kowalewski, Fluid Dyn. Res. **17**, 121–145 (1996).
[13] W. von Ohnesorge, Z. Angew. Math. Mech. **16**, 355–358 (1936).
[14] X. D. Shi, M. P. Brenner, and S. R. Nagel, Science **265**, 157, (1994).
[15] Y. J. Chen and P. H. Steen, J. Fluid Mech. **341**, 245–267 (1997).
[16] R. F. Day, E. J. Hinch, and J. R. Lister, Phys. Rev. Lett. **80**, 704 (1998).
[17] D. T. Papageorgiou, Phys. Fluids **7**, 1529 (1995).
[18] C. M. Bender and S. A. Orszag, Advanced Mathematical Methods for Scientists and Engineers (Mc Graw-Hill, New York, 1978).
[19] A. U. Chen, P. K. Notz, and O. A. Basaran, Phys. Rev. Lett. **88**, 174501,1–4 (2002).
[20] A. Rothert, R. Richter, and I. Rehberg, New J. Phys. **5**, Art. No. 59 (2003).
[21] J. R. Lister and H. A. Stone, Phys. Fluids **10**, 2758–2764 (1998).
[22] J. M. Rallison and A. Acrivos, J. Fluid Mech. **89**, 191–200 (1978).
[23] I. Cohen, et al., Phys. Rev. Lett. **83**, 1147–1150 (1999).
[24] A. Sierou and J. R. Lister, J. Fluid Mech. **497**, 381–403 (2003).
[25] P. Doshi et al., Science **302**, 1185–1188 (2003).
[26] M. Moseler and U. Landmann, Science **289**, 1165–1169 (2000).
[27] J. Eggers, Phys. Rev. Lett. **89**, 084502, 1–4 (2002).
[28] S. L. Anna and G. H. McKinley, J. Rheol. **45**, 115–138 (2001).
[29] Y. Amarouchene, D. Bonn, J. Meunier, and H. Kellay, Phys. Rev. Lett. **86**, 3558–3561 (2001).

© 2005 WILEY-VCH Verlag GmbH & Co. KGaA, Weinheim